

## Stimulated Creation of the SOI Structures with Si nano-clusters by low-dose SIMOX Technology

V. Litovchenko\*, B. Romanyuk, V. Melnik, V. Klad'ko, V. Popov,  
O. Oberemok and I. Khatsevich.

V. Lashkaryov Institute of Semiconductor Physics, NAS of Ukraine, 41 Prospekt Nauki, Kyiv,  
03028, Ukraine; \*Tel/Fax: +(38044) 525-62-90, e-mail: [lvlg@isp.kiev.ua](mailto:lvlg@isp.kiev.ua)

**Keywords:** silicon, nanocluster, buried layer, ion implantation, defects

**Abstract.** The peculiarities of a buried layer formation obtained by a co-implantation of O<sub>2</sub> ions with the energy of 130 keV and carbon ions within the energy range of 30-50 keV have been investigated. The corresponding ion doses for carbon and oxygen ions were equal to  $2 \cdot 10^{16} \text{ cm}^{-2}$  and  $1.8 \cdot 10^{17} \text{ cm}^{-2}$ , respectively. It has been observed that annealing at 1150°C results in enhanced oxygen diffusion towards the region with a maximum carbon concentration. Analysis of x-ray diffraction patterns and TEM images confirm formation of Si nanoclusters in the SiO<sub>2</sub> buried layer. The intensive luminescence with the maximum at 600 nm has been observed in the synthesized structures.

### Introduction

The silicon on insulator (SOI) structures with embedded Si nano-clusters are perspective for memory, MOS-transistors, high-frequency tunneling diodes and other devices, including nanoelectronic devices. The SIMOX technology is, as known, very reliable and programmable one, but conventional regime needs very high doses and high annealing temperature.

In our previous works [1, 2] proposed, to avoid these difficulties, the two approaches: stimulation factor, which promote the SiO<sub>2</sub> creation of the indicated thickness, and low-dose oxygen implantation. The SiO<sub>2</sub> formation were enhanced by carbon implantation inside the buried oxygen-enriched layer (O<sub>2</sub><sup>+</sup> pre-implantation) and subsequent annealing.

Perfect SiO<sub>2</sub> layer formed by this stimulated technology have been demonstrated very good insulator properties.

Other task arises – creation by this technology of Si-nanoclusters embedded in SiO<sub>2</sub> buried layer Silicon nanocrystalline particles (nc-Si) studied for application in micro- and optoelectronic devices (light-emitting devices, memory cells, etc) [3]. For silicon nanocrystal synthesis the annealing of non-stoichiometric silicon oxide (SiO<sub>x</sub>) films [4,5] or SiO<sub>2</sub>-Si structures, implanted by silicon ions [6,7] are used. At the buried SiO<sub>2</sub> film formation by SIMOX (silicon implanted by oxygen) technology it was shown that the films contain silicon inclusions [8].

As a rule the dimensions of such inclusions are within the range of 10 to 100 nm, and the use of those for light emission is impossible. At the same time synthesis of the buried insulating layers containing silicon nanocrystals has the perspectives of a practical use in the multi-layer optoelectronic circuits.

In the present work influence of the additional carbon implantation on silicon nanocluster formation in the buried oxide (BOX) layer was investigated using the set of experimental methods.

## Materials and Methods

All the silicon samples (n-type, 100 orientation) were implanted by  $O_2^+$  ions (energy 130 keV, doses  $1.8 \cdot 10^{17}$ ,  $2 \cdot 10^{17}$  and  $5 \cdot 10^{17} \text{ cm}^{-2}$ ). Part of the samples was implanted by carbon ions with energy 30 keV (dose  $1 \cdot 10^{16} \text{ cm}^{-2}$ ) or 50 keV (dose  $2 \cdot 10^{16} \text{ cm}^{-2}$ ). Furnace annealing was carried out at  $1150^\circ\text{C}$  or  $1200^\circ\text{C}$  in argon ambient for 20 minutes.

Investigation of the peculiarities of defect creation and transformation were carried out by the X-ray diffuse scattering (XDS) technique using the high-resolution diffractometer PANalytical X'Pert Pro MRD.

The XDS intensity distribution  $I(\mathbf{q})$  was measured in the vicinity of the 004 node. The  $\mathbf{q}$  vector components in the diffraction plane are connected with the experimental conditions by the following expression:

$$(q_z, q_x) = (\eta \cos \vartheta_B (2\Delta\alpha - \Delta\eta) \sin \vartheta_B) / \lambda \quad (1)$$

where  $\lambda$  is the X-ray wavelength,  $\eta$  and  $\Delta\alpha$  – angle deviations of the analyzer and monochromator, correspondingly,  $\vartheta_B$  – the Bragg angle, the Z axis is directed normally to the surface, and the X axis is parallel to the sample surface; these angles are disposed within the diffraction plane.

The method of determination of micro-defect (MD) concentration consists in determination of the ratio of the Huang and thermo-diffuse scattering, excepting influence of the thickness of scattering layer, structure amplitude, corporal corner of scattering, and Debye-Waller factor. So, such important parameters as the micro-defect symmetry, dimension, and concentration may be directly determined from experimental data according diffuse scattering for the sample investigated.

Distribution of the dopants was investigated by secondary ion mass spectrometry (SIMS) by Cameca IMS 3F. Photoluminescence (PL) spectra were measured after the plasma ion etching of the top Si layer at excitation by helium-cadmium laser ( $\lambda=325 \text{ nm}$ ). Thickness and position of the BOX layer were investigated by the transmission electron microscopy (TEM) in a cross-section mode.

## Results and discussion

Fig. 1 shows oxygen depth distribution for samples before and after post-implantation annealing (implantation doses  $2 \cdot 10^{17} \text{ cm}^{-2}$  and  $5 \cdot 10^{17} \text{ cm}^{-2}$ ). At low implantation dose (Fig.1a) nucleation and growth of the  $\text{SiO}_2$  phase goes both at the region of oxygen maximum concentration, and at the region of vacancy accumulation. Buried  $\text{SiO}_x$  layer splits to the two parts with intermediate Si-enriched interlayer. It leads to formation of non-compact  $\text{SiO}_2$  layer with inclusions of non-oxidized silicon. At annealing of the samples implanted by  $O_2$  with a dose  $5 \cdot 10^{17} \text{ cm}^{-2}$  stoichiometric oxide layer with sharp Si- $\text{SiO}_2$ -Si interfaces is formed (Fig 1b).

Profiles of oxygen atom distribution for the samples after oxygen ion implantation and combined implantation by oxygen and carbon ions after annealing at  $T=1150^\circ\text{C}$  are shown in Fig.2.

After oxygen implantation and annealing at  $1150^\circ\text{C}$  the oxygen distribution profile coincides with the calculated (by the TRIM software) one. After additional carbon implantation (50 keV) the oxygen distribution profile shifts to the sample surface, and is placed in the region between the maximum of carbon distribution at given energy and maximum of vacancy concentration created at oxygen implantation. For the samples additionally implanted by carbon with the energy of 30 keV it is observed the region of  $\sim 30 \text{ nm}$  depth with a constant oxygen concentration that is an evidence of creation of thin stoichiometric  $\text{SiO}_2$  layer.

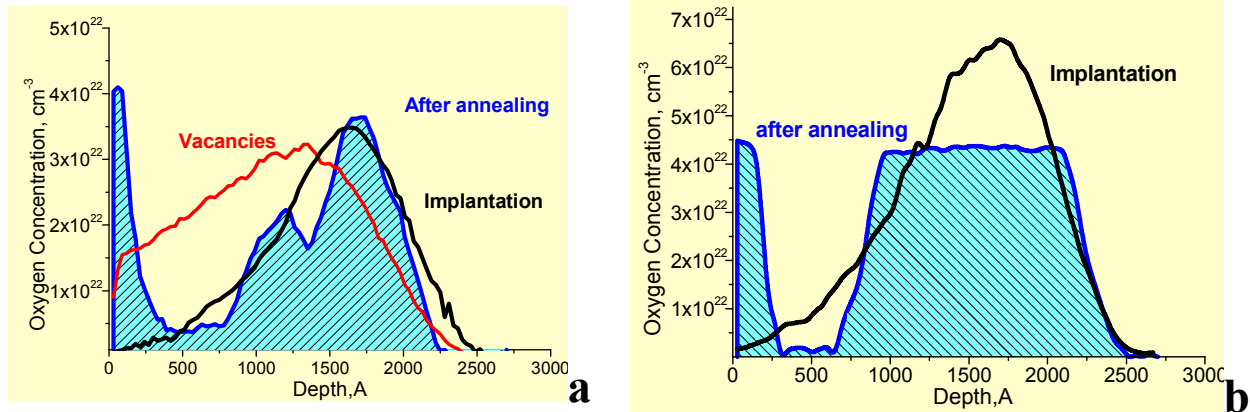


Fig.1 Oxygen depth distribution for samples before (line) and after post-implantation annealing at 1200°C (shaded area) for implantation doses  $2 \cdot 10^{17} \text{ cm}^{-2}$  (a) and  $5 \cdot 10^{17} \text{ cm}^{-2}$  (b)

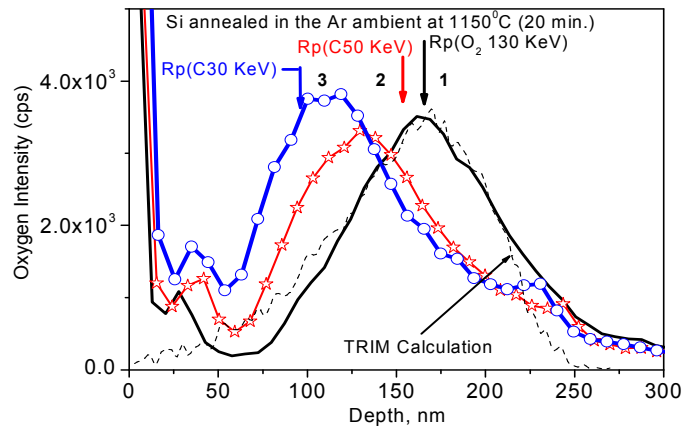


Fig.2. Oxygen depth distribution after annealing for the samples implanted by oxygen (1), and additionally implanted by carbon ions with the energies of 50 keV (2) and 30 keV (3)

Cross-section TEM and LEED images of the sample after oxygen implantation (a), and additional carbon implantation (b) are shown in Fig.3.

The buried oxide layer of the samples additionally implanted by carbon is noticeably thinner (correlates with SIMS data, Fig.2). HRTEM image shows that after thermal annealing for the samples implanted by oxygen only, Si- nanocrystalline inclusions with dimensions of 10 to 30 nm in buried oxide layer are present. For the carbon co-implanted samples nanocrystal dimensions substantially decrease up to 3 – 10 nm.

The XDS curves for the samples after oxygen implantation (curve 1), carbon co-implantation (curve 2), and after annealing of these samples (curves 3, 4) are presented in Fig.4.

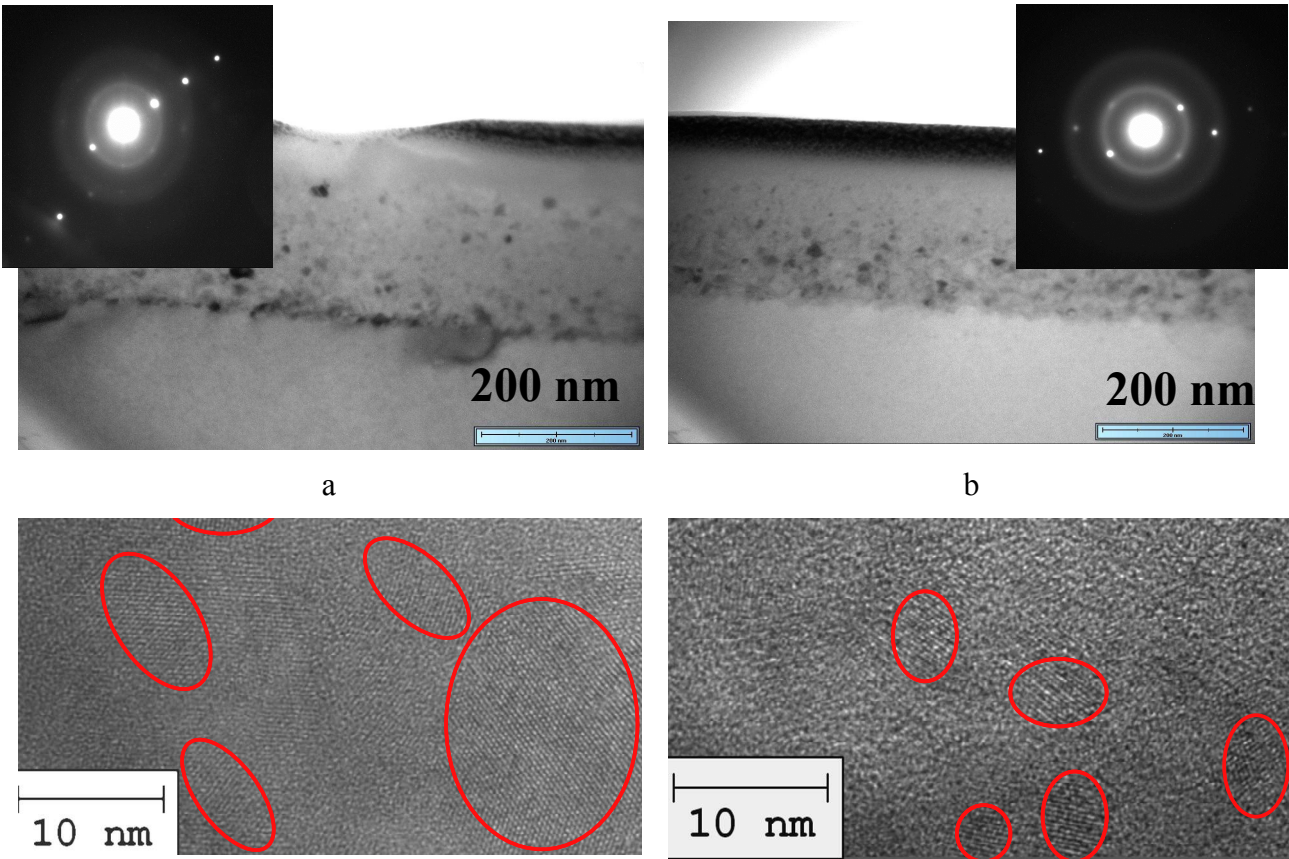


Fig. 3. Cross-section TEM and LEED images of oxide layer for oxygen only implanted sample (a) and carbon co-implanted sample (b) and HRTEM image of Si nanoclusters in the SiO<sub>2</sub> layer.

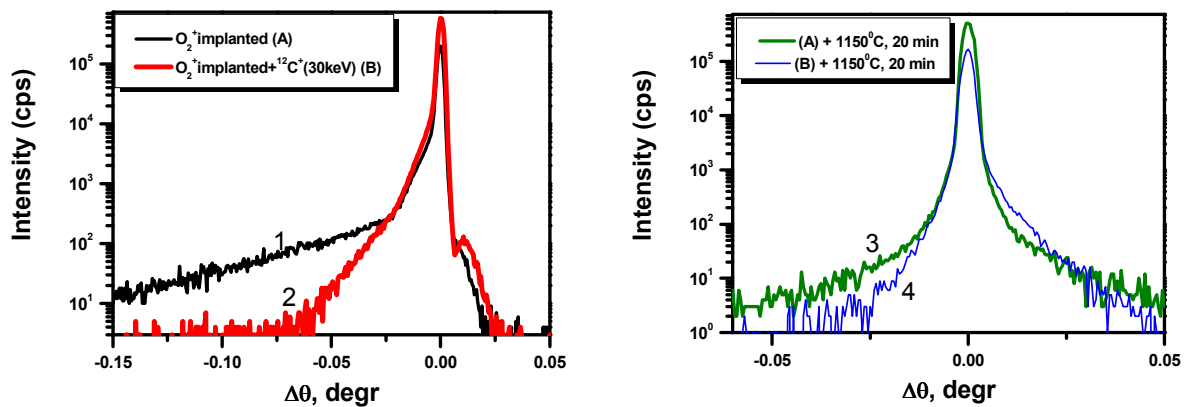


Fig. 4. The XDS curves for the samples after oxygen implantation (curve 1), carbon co-implantation (curve 2), and after annealing of these samples (curves 3, 4).  $\Delta\theta = \vartheta - \vartheta_B$ .

Half-width of the XDS maximum represents the integral characteristic of crystal perfection, and is of 5.6 angle sec. It is very close to the theoretical value, and testifies the sample perfection. We have used the diffusing scattering method to obtain the MD parameters. Picture of the diffusing scattering distribution in the direction parallel to reciprocal lattice vector ( $q_z$ -section) is shown in Fig. 4, where  $q$  – vector from the reciprocal lattice knot to the measuring point for implanted samples before and after annealing.

$I(\mathbf{q})$  distribution shapes indicate that all the samples include the MDs as vacancy ( $q_z < 0$ ) and interstitial ( $q_z > 0$ ) types. Fig.4 shows that the  $I(\mathbf{q})q^2$  normalized intensity is not identical for all  $q_z$  region. It means that the scattering are realized in the asymptotic area where the defect power  $C$  is proportional to the  $q \gg (\mathbf{Q}C)^{-1/2}$ .  $\mathbf{Q}$  – the reciprocal lattice vector.

The  $I(\mathbf{q})$  distribution indicates that all the samples have the MD both of vacancy ( $q_z < 0$ ), and interstitial ( $q_z > 0$ ) type. One can see from Fig. 5 that the normalized intensity  $I(\mathbf{q})q^2$  is not similar for all the  $q_z$  interval. It means that scattering takes place in the asymptotic region, where the defect power  $C$  is proportional to  $q \gg (\mathbf{Q}C)^{-1/2}$ . Here  $\mathbf{Q}$  is the vector of reciprocal lattice. It is easily to obtain the MD dimensions from the coordinates of the point of transition to horizontal character of the scattering dependence. The samples before annealing are characterized by high MD concentration ( $> 10^{11} \text{ cm}^{-3}$ ) with the dimensions of  $\sim 10$  to  $1000 \text{ nm}$ . Scattering intensity values for the samples before annealing for the negative  $q_z$  are substantially higher than for the positive ones. It means that the total capacity of the vacancy-type MD is higher (approximately 2 times) than of the interstitial ones.

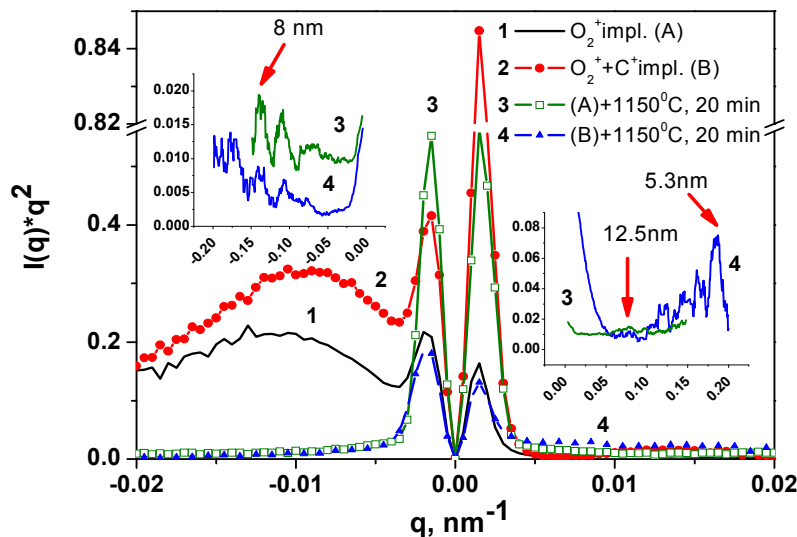


Fig.5 Dependence of the normalized intensity  $I(\mathbf{q})q^2$  on  $\mathbf{q}$  vector: for  $\text{O}_2^+$  implanted Si before (curve 1) and after (curve 3) annealing; for  $\text{O}_2^+$  implanted Si with additional  $\text{C}^+(30\text{keV})$  implantation in the vacancy region before (curve 2) and after (curve 4) annealing.

After ion implantation substantial diffuse scattering in the region of negative angles is observed in the XDS curves. It points out the great concentration of the vacancy defects. Carbon implantation leads to the substantial scattering decrease in the region of negative  $q_z$  owing to vacancy trapping of carbon atoms. At that it is observed scattering in the region  $q_z > 0$  that is caused by interstitial component due to additional incorporation of interstitial atoms at carbon implantation, and compensation of stretching tensions in the sub-surface region.

After annealing it is observed substantial decrease of the diffuse scattering. For the additionally carbon-implanted samples the scattering component at  $q_z > 0$  is some higher than for the samples, implanted only by oxygen.

During oxygen-implanted sample annealing the  $\text{SiO}_2$  phase is forming. Excess silicon atoms recombine with vacancies in the region closer to the surface, also interstitial defect complexes behind the implantation region are created (see Fig.3). As a result a buried non-continuous  $\text{SiO}_2$  layer with inclusions of silicon crystallites (10 to 100 nm dimensions) is formed. It is confirmed by the XDS results.

In the case of additional carbon implantation the SiO<sub>2</sub> phase rise occurs in the region of carbon implantation and profile of oxygen distribution shifts to the surface. It is connected with the two factors: in the region of carbon distribution the critical radius of SiO<sub>2</sub> precipitates is noticeably less, that creates the conditions for effective rise of SiO<sub>2</sub> phase; drains for interstitial atoms are present that decrease precipitation velocity in the region of initial oxygen distribution.

The diffuse scattering distribution for the  $q_x$ -curves shows that the displacement fields are close to the spherical ones. For the samples after annealing it is observed continuous spectrum of small-size defects (from nanometers up to few ten nanometers).

PL spectra for the oxygen implanted and carbon co-implanted samples are shown in Fig.6. After oxygen implantation the PL intensity in the region of 400 to 800 nm is rather small. For the carbon co-implanted samples it is observed the intensive PL band with a maximum at 600 nm. Shape of this band is a complex one and may be approximated by a few Gauss curves, which can be related to luminescence of Si-nanocrystals with the sizes 2-5 nm.

The presence of such Si-nanocrystalline inclusions in the thin stoichiometric SiO<sub>2</sub> layer is confirmed by our XDS results, which is formed in the samples implanted by oxygen and carbon.

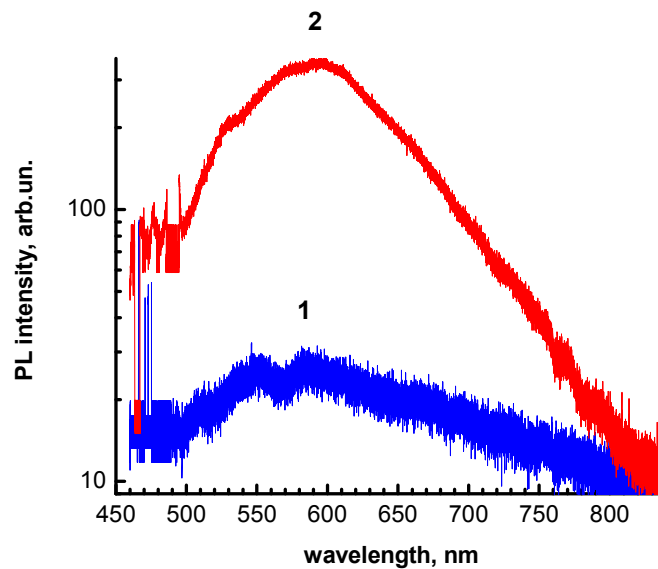


Fig. 6. PL spectra of annealed samples implanted by oxygen (1), and co-implanted by carbon (2)

Enhancement of the Si precipitation in spherical clusters under carbon implantation can be described in the framework of the nucleation model, proposed by J. Vanhellemon and C. Claeys [9]. In this model the change of the Gibbs free energy  $\Delta G$  was associated with the formation of the spherical Si-cluster with radius  $R_j$  [10,11]. Additional non-equilibrium vacancy  $V$  (interstitial – I) impurity or defects lead to opposite influence on Si-precipitate growth: enhancement – for vacancy type of mixtures, or suppression – for interstitial particles:

$$N_{pre} = N_C \left( \frac{V}{V^0} \right)^{-\beta} \left( \frac{I}{I^0} \right)^{\gamma}, \quad \beta, \gamma > 0 \quad (2)$$

i. e. the growth of Si cluster has a strong exponential dependence on the number of vacancy-like inclusions. In this expression,  $\beta$  and  $\gamma$  are the numbers of vacancies and Si interstitials taking part in the precipitation process per one incorporated Si atom.

Another mechanism of carbon influence is an effect of quasi-chemical (catalytic) reactions:

1.  $[\text{Si} + \text{C} + \text{O}_2] \rightarrow \text{SiO} + [\text{CO}] \rightarrow [\text{SiO}_2] + \text{C}$  -  $\text{SiO}_2$  phase formation
2.  $n[\text{Si}] + \text{V}(\text{C}) \rightarrow \text{Si}_n$  - Si cluster formation.

As a result the Si nanocluster formation is energetically efficient.

The results obtained are explained within the framework of the model of stimulated creation of the Si-enriched buried layer. For this model and calculations the catalytic action of carbon during  $\text{SiO}_2$  layer and Si cluster formation are considered as principal points.

## Conclusions

The low-dose SIMOX with  $\text{C}^+$  co-implantation was investigated. It was demonstrated that after annealing of carbon co-implanted samples the interstitial defect concentration increases, and those condense to Si nanoclusters.

It is shown that additional implantation of carbon ions in silicon structures, pre-implanted by oxygen leads to redistribution of oxygen with the depth, and stimulates  $\text{SiO}_2$  phase creation in the region maximum carbon concentration. This effect enhances when the carbon distribution coincides with the maximum of vacancies distribution.

Thus the carbon introduction allows effectively control the nucleation of silicon nanoclusters and the growth of  $\text{SiO}_2$  phase during annealing. Conditions for the efficient formation of nanoclusters (3-10 nm) silicon in the  $\text{SiO}_2$  film are realized. For such structures the intensive PL with a maximum at 600 nm are observed.

## Acknowledgements

Financial support by the Ministry of Education and Science of Ukraine (Grant M/90-2010) and Project 3.5.1.28 SP is gratefully acknowledged.

## References

1. V.G. Litovchenko, A.A. Efremov, B.N. Romanyuk, V.P. Melnik and C. Claeys. Use of gettering and defect induced processes in ultra-thin buried oxide synthesis. *Solid State Phenomena*, 1997, V. 57-58, p.97-102.
2. N.I. Klyui, V.G. Litovchenko, B.N. Romanyuk, V.P. Melnik, V.G. Popov, Extended Abstracts, Spring meeting, San Francisco, California, 1994, May 22-27, V. 94-1, p. 876.
3. Sandip Tiwari, Farhan Rana, Hussein Hanafi, et al. A silicon nanocrystals based memory. *Appl. Phys. Lett.*, 1996, 68(10), 1377-1379.
4. B.N. Romanyuk, V.P. Melnik, V.G. Popov, I.M. Khatsevich, A. S. Oberemok. Influence of low-temperature annealing on the photoluminescence of silicon nanocluster structures. *Semiconductors*, 2010, 44 (4), 533-537.
5. T. Inokuma, Y. Wakayama, T. Muramoto, et al. Optical properties of Si clusters and Si nanocrystallites in high-temperature annealed  $\text{SiO}_x$  films. *Journal of Applied Physics*. 1998, V. 83, p. 2228-2234.
6. A. Romanyuk, V. Melnik, Ya. Olikh, J. Biskupek, U. Kaiser, M. Feneberg, K. Thonke, P. Oelhafen. Light emission from nanocrystalline silicon clusters embeded in silicon dioxide: role of the suboxide states. *Journal of Luminescence*, 2010, 130, 87
7. T. Shimizu-Iwayama et al "Optical properties of silicon nanoclusters fabricated by ion implantation" // *J. Appl. Phys.*, 1998, v. 83, №11, pp. 6018-6022.

8. A. Nejim, Y. Li, C.D. Marsh, P. L. F. Hemment, R. J. Chater, J. A.. Kilner, and G. R. Booker. Direct formation of device worthy thin film SIMOX structures by low energy oxygen implantation. *Nuclear Instr. & Methods in Physics Res.*, **1993**, B80/81, 822-826.
9. J. Vanhellefont and C. Claeys. A theoretical study of the critical radius of precipitates and its application to silicon oxide in silicon. *J. Appl. Phys.* 1987. **62**, 3960.
10. C. Claeys and J. Vanhellefont, in Proc. 2nd “Gettering and Defect Engineering in the Semiconductor Technology” GADEST-87, ed. H. Richter, p. 3.
11. A. Sarikov, I. Lisovskyy, V. Litovchenko, M. Vitovich, S. Zlobin, et al. Mechanisms of oxygen precipitation in Cz-Si wafers subjected to rapid thermal anneals. *Journal of the Electrochemical Society*, 2011, V.158 (8), p.772-777.

## **Gettering and Defect Engineering in Semiconductor Technology XIV**

doi:10.4028/www.scientific.net/SSP.178-179

## **Stimulated Creation of the SOI Structures with Si Nano-Clustersw by Low-Dose SIMOX Technology**

doi:10.4028/www.scientific.net/SSP.178-179.17